Received: 30 August 2021 | Revised: 12 April 2023 | Accepted: 14 April 2023

DOI: 10.1002/esp.5602

RESEARCH ARTICLE

ESPL WILEY

Contribution of bedrock structures to the bedrock surface topography and groundwater flow systems within deep glaciofluvial aquifers in Kurikka, Western Finland

Eemi Ruuska[1] | Pietari Skyttä[1] | Niko Putkinen[2] | Tuire Valjus[3]

[1]Geology Section, Department of Geography and Geology, University of Turku, Turku, Finland

[2]Geological Survey of Finland, Kokkola, Finland

[3]Geological Survey of Finland, Espoo, Finland

Correspondence
Eemi Ruuska, Geology Section, Department of Geography and Geology, FI-20014 University of Turku, Finland.
Email: eeolru@utu.fi

Funding information
Maa- ja Vesiteksiikan Tuki Ry, Grant/Award Number: 13-7820-39

Abstract

One of the key challenges related to glaciofluvial aquifers is understanding how the underlying bedrock structures and the associated bedrock surface topography contributed to the deposition of the glaciofluvial sediments and the generation of groundwater flow pathways. In this study from Western Finland, we present a new digital elevation model of the Precambrian crystalline bedrock surface buried up to 100 m beneath the glaciofluvial sediments along the Kurikka depression. We link bedrock topography to structural anisotropy using additional data from rock outcrops, boreholes and gravity data. Brittle deformation zones are seen in the bedrock-digital elevation model (DEM) as sharp breaks in the rock surface. These vertical fracture zones contributed to the development of interlinked elongate bedrock depressions and delimit rock blocks with different elevations. A narrow, zigzagging trench, with a stepped floor, follows WNW-ESE and NE-SW oriented fracture zones and forms a major hydraulic connection between two major parts of the aquifer. Furthermore, the conductive fracture zones are conduits which connect the shallow glacifluvial aquifer system to deep groundwater in the bedrock. Understanding bedrock structures and buried topography is critical for successful groundwater modelling in crystalline, fractured bedrock.

KEYWORDS
aquifer, deformation zone, DEM, structural geology, topography

1 | INTRODUCTION

Groundwater flow within glacial drift aquifers is known to depend not only upon the thickness, physical properties and internal structure of the Quaternary sediments but also on the topography of the underlying bedrock (e.g. Godbout et al., 2011) and the hydraulic connectivity between the bedrock and the overlying glaciofluvial deposits (Cassidy et al., 2014; Kempton et al., 1991; Lipponen, 2006). Despite the recognised role of the bedrock, systematic analysis of the bedrock structures as a base layer for the glacial deposits has been frequently overlooked in regional aquifer modelling, with exceptions, for example, on the Canadian Shield (DesRoches et al., 2014; Gao, 2011; Gleeson & Novakowski, 2009; Richard & Chesnaux, 2014; Steelman et al., 2018). For this reason, digital elevation models representing the bedrock surface (hereafter bedrock-DEM) and acting as the depositional basement for the glaciofluvial aquifers do not always adequately honour the bedrock structure. Moreover, most existing geological and hydrological models lack sufficient understanding of the linkage between the crystalline basement and the sediment cover. Bedrock structures contribute to the bedrock-DEM morphology, but brittle deformation zones within the crystalline bedrock also provide groundwater flow pathways which largely define the hydrogeological conductivity of the bedrock. Distributed flow along individual planar discontinuities may be localised into channelised pathways (Brown et al., 1998; Sanderson & Peacock, 2019; Stephens et al., 2015) generated by interlinked linear 'tubes' of pronounced conductivity within

fault bends, intersections and step-overs (Cox, 1999; Dimmen et al., 2017; Micklethwaite et al., 2015; Peacock et al., 2018).

In this paper, we show that the bedrock structure and surface morphology play a much more fundamental role in governing the groundwater flow in large-scale glaciofluvial aquifers than previously considered. Specifically, zones of brittle deformation act as high permeability conduits, as well as contribute to the generation of bedrock depressions, which further localise groundwater flow into channelised networks. Further, we show that even limited datasets of the bedrock structure available from poorly outcropping areas are useful in addressing the morphology of the bedrock surface topography.

We conducted the investigation within the Kurikka buried valley aquifer complex, Western Finland (Figure 1). The aquifer complex is characterised by laterally extensive coarse-grained sediment assemblages comprising alternating layers of till, with significant groundwater resources comparable with the buried valley aquifers in Canada (Ross et al., 2005; Russell et al., 2004). At large scales, deposition of the subglacial sediments is controlled by the ice sheet thickness, glacier bed and ice sheet topography (Benn & Evans, 2010; Boulton, 1986; Boulton et al., 2001; Lovell et al., 2011; Shreve, 1972, 1985) which govern both the localisation and the stratigraphy of the deposits. Furthermore, spatial association between individual glaciofluvial deposits and bedrock structures such as brittle fractures and lithological contacts and particularly the morphologic features they induced upon the bedrock surface have been recognised (Barr & Lovell, 2014; Burbank & Fort, 1985; Okko, 1962; Palmu, 1999; Skyttä et al., 2015; Sugden & John, 1976). Brittle structures have a direct linkage to the hydrogeology by the groundwater filling the pore spaces of the sediment and rock. Those voids play the major role in this type of aquifer system. Recent (Putkinen et al., 2020; Putkinen et al., 2012; Rashid et al., 2020) and ongoing studies by the Geological Survey of Finland (GTK) in Kurikka have shown that the volume

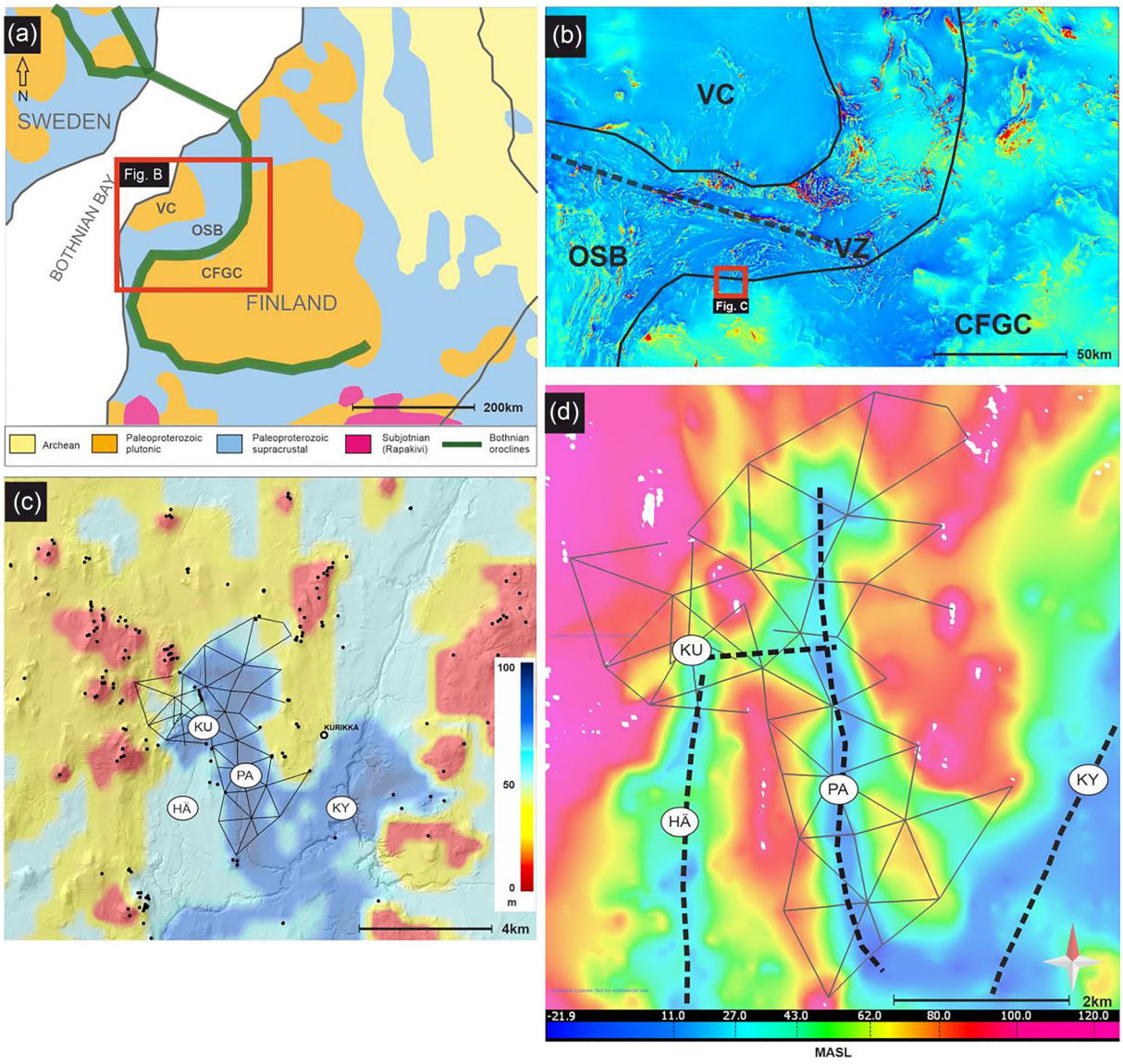

FIGURE 1 (a) Generalised bedrock map of Central Finland; Bothnian Oroclines after Lahtinen et al. (2017). (b) Aeromagnetic map (GTK) of western Finland. CFGC, Central Finland Granitoid Complex; Ostrobothnia Schist Belt; OSB, Ostrobothnia Schist Belt; VC, Vaasa Complex; VZ, Vittinki Zone. (c) Hill-shaded ground surface topography (LiDAR) and soil cover thickness (color-coded; GTK). Locations of bedrock geological observations are marked as black dots and black solid lines represent gravimetric survey lines. HÄ, Häjyluoma; KU, Kuusistonloukko; KY, Kyrönjoki; PA, Paloluoma. (d) Bedrock surface digital elevation model (DEM) of the Paloluoma and Kuusistonloukko (highlighted as black dashed lines) based on gravimetric and borehole data (Putkinen et al., 2012).

and hydrogeological properties of the Quaternary deposits alone cannot explain the large amount of groundwater recharge and that some of the bedrock depressions with fractures likely provide hydrogeological linkages between different parts of the aquifer. However, the bedrock structure has not been accounted for when interpolating the bedrock-DEM from dominantly gravity data, a typical dataset used in bedrock surface modelling (Møller et al., 2007; Steelman et al., 2018), and no further investigations on the bedrock structure have been conducted.

In this study, we addressed the relationship between the bedrock structure and bedrock surface topography through conducting structural analysis of the bedrock within the main recharge area of the Kurikka aquifer system (Figure 1c). We used the results to reinterpret the morphology of the existing bedrock-DEM which was previously generated without utilizing the structural information of the bedrock. We placed specific attention upon recognition of steeply dipping zones within the bedrock-DEM which likely reflect the presence of discrete vertical to sub-vertical deformation zones but where the surface geometries are not realistically represented due to the characteristic smooth, curvilinear shape of the bedrock surface interpretation derived from gravity data. Subsequently, we re-interpreted the gravity data from selected survey lines and used the revised interpretation together with the field observation data in modifying the bedrock-DEM to better honour the character of the structure of the bedrock. We also mapped bedrock lineaments from ground surface DEM for the regional scale comparison. Moreover, we generated a 3D-photogrammetric model from a bedrock outcrop in the study area to illustrate the effect of a discrete shear zone and associated fracturing on the topography of the bedrock surface and compare the results with the improved bedrock-DEM to reduce the conceptual uncertainty of the models.

2 | GEOLOGY OF THE STUDY AREA

The western and southern parts of the study area (Figure 1a,b) comprise post-kinematic, largely undeformed 1.88–1.87 Ga granodioritic–granitic–dioritic intrusive rocks of the Central Finland Granitoid Complex (CFGC) (Nikkilä et al., 2016; Nironen et al., 2000). The northern and eastern parts of the study area comprise supracrustal 1.90–1.89 Ga rocks of the Ostrobothnia Schist Belt (OSB). OSB is lithologically dominated by biotite paragneisses and structurally characterised by the ENE-WSW striking, dextral Vittinki high-strain zone (Pääkkönen, 1966) occurring approximately 30 km north of the study area and NE-SW striking ductile shear zones abutting the Vittinki zone at the central parts from the Southwest (Figure 1b; Vaarma & Kähkönen, 1994; Lehtonen et al., 2005). Structural signatures within the study area and its surroundings have been attributed to the coupled Bothnian oroclines (Lahtinen et al. (2017) bounded by the migmatitic Vaasa Complex (VC; Chopin et al., 2020) in the west and the CFGC in the east (Figure 1a).

The bedrock of the study area is characterised by negligible variability in overall topography and ultra-slow erosion of <2.5 m/Ma as revealed by tiered unconformities and impact structures (Hall et al., 2021). However, the presence of Mesoproterozoic sedimentary rocks comparable with the sandstones in the Bothnian Sea and Satakunta half-graben (Pokki et al., 2013) is found within the 100-m-deep valley systems in Ostrobothnia and point towards the presence of long-lived valleys since 1.5 Ga (Hall et al., 2021). In Kurikka area, the bedrock surface morphology is characterised by one major elongate NNE-trending depression located within the Kyrönjoki river valley (KY in Figure 1c) and minor but distinct depressions beneath the approximately NNW-SSE-trending Paloluoma (PA) and Häjyluoma (HÄ) Valleys. Since their formation, a long burial history persisted until the valleys were finally exhumed at about 40 Ma ago (Gibbard & Lewin, 2016). Since then, the evolution is controlled by the river system operation across the Late-Paleocene and Neogene periods while the Pleistocene glaciers made the final touch-up for the first- and second-order valley morphologies. Besides the larger depressions, a connective E-W-trending depression at Kuusistonloukko (KU) occurs in-between the HÄ and PA depressions and has been considered to provide hydrogeological linkage of aquifers associated with the HÄ and PA depressions (Putkinen et al., 2012). However, the character of the depression is so far unknown. Even smaller valleys are present in the Lehtivuori–Karhuvuori areas (third-order valleys).

Buried valleys are filled dominantly during the last Weichselian deglaciation at approximately 11.5–10.5 Ka (Putkinen et al., 2020). However, Pitkäranta (2009) suggests that deepest sedimentary deposits in the valleys are potentially filled even as early as during the Middle or Early Pleistocene. The deglaciation dynamics of the region involved an interplay between the Western Finland ice lobe in the east and a domain of passive ice in the west, and this interlobate setting with lateral margin deposition is characterised by accumulation of large amount of sediments and overall weak glacial erosion (Putkinen et al., 2017; Figure 2). The post-glacial superficial Quaternary deposits in the area include basin sediments such as clays and silts and extensive littoral deposits that were formed to higher-standing areas during the following thousands of years of land uplift and subsequent exposure to strong currents and wave activity in shallow water starting about 10.5 Ka ago.

The Quaternary deposits of the study area (Figure 2a) are both laterally and vertically extensive and reach a thickness of over 100 m in the PA Valley which hosts the main aquifers of the study area. The PA aquifer consists of three partially overlapping major aquifers located at depths of 15–20 m, approximately 40–70 m and approximately 70–85 m below the ground level (Figure 2b; Putkinen et al., 2012). The aquifers typically comprise permeable medium-grained sands, but also, fine gravel occurs in the deepest aquifer resting on till or fractured bedrock. The topmost impermeable clay and fine silt sediments form a pressurised character to the groundwater of the valley (Putkinen et al., 2012; Figure 2d). However, subsequent studies have shown that aquifers, particularly in the KU-PA area, are more complex in character than the conceptual diagram of the sediment stratigraphy (Figure 2b) indicates.

Infiltrated groundwater recharge routes from the topographically higher areas (in the west) to the aquifers are controlled by the atmospheric pressure and gravity, and the ground elevation difference of over 100 m from the main recharge area to the destination of aquifer areas constitutes up to 100-m difference to the potentiometric surface for the groundwater that has artesian character in sediments and bedrock. In the KU depression, Putkinen et al. (2012) attributed the hydrogeological connectivity of the different aquifer parts to the presence of the conductive middle sand horizon. Putkinen et al. (2012) also recognised the role of the bedrock fracture zones as potential

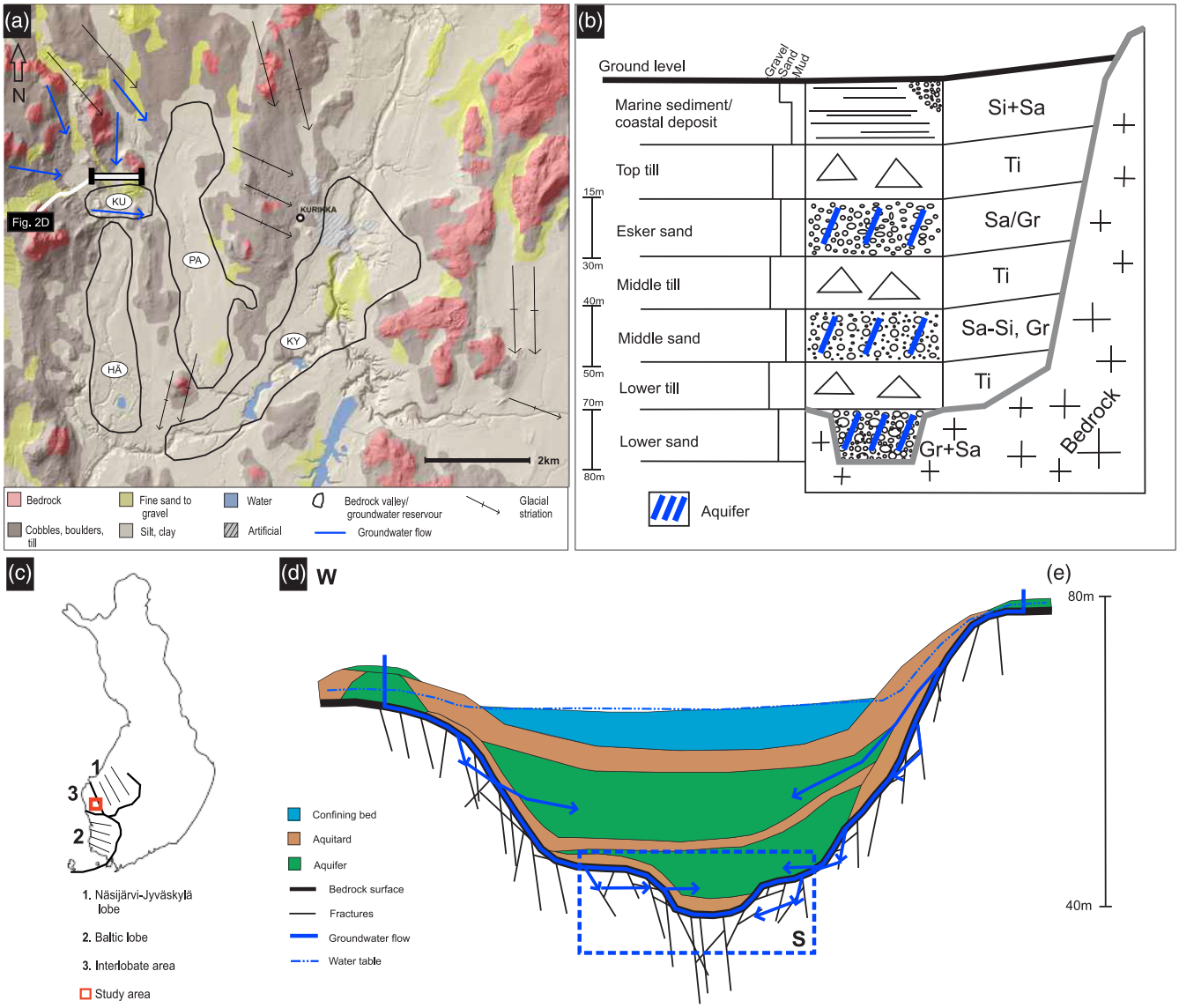

FIGURE 2 (a) Map of surface Quaternary deposits map in the study area by National Land Survey (NLS) with hill-shaded ground surface topography (LiDAR; GTK). B) a schematic stratigraphic column of Quaternary deposits within the Paloluoma Valley (modified after Putkinen et al., 2012). Gr, gravel; Sa, sand; Si, silt; Ti, till. (c). Index map showing the glacial lobe areas of western Finland and the location of the study area (red box). (d) Kuusistonloukko confined aquifer system recharge is characterised by downcasting flowing groundwater on the sides of the valley filling sediment aquifers. The main aquifer is situated in the base of the valley (blue box), where the interplay of the bedrock fractures and overlying porous sedimentsare considered to govern the groundwater flow.

carriers of groundwater, and recent finite element groundwater flow modelling (Rashid et al., 2020) has further confirmed that flow systems within the Kurikka aquifer system are complex, and the bedrock and its fracture zones apparently have a major role in controlling the inflow and maintaining the groundwater system (Figure 2d).

3 | DATA AND METHODS

Understanding the brittle bedrock structures in areas of limited outcrop must be primarily developed using conceptual models over the regional fracture patterns, with particular focus on the zones of localised brittle deformation (faults, fracture zones) comprising intensely fractured cores and surrounding damage zones (DZs) (Childs et al., 2009; Kim et al., 2004; Peacock et al., 2017). Further, lithological composition of the crust, structural inheritance from older (ductile) structures and reactivation of older deformation zones will likely contribute to the generation of brittle structures, including the architecture of the fault zones (Korme et al., 2004; Mancktelow & Pennacchioni, 2005; Pizzi & Galadini, 2009; Skyttä et al., 2021; Skyttä & Torvela, 2018), and should hence be studied to decrease the uncertainties related to the build-up of the brittle structural model.

Bearing in mind the above, we conducted systematic analysis of the ductile and brittle structures of the bedrock within the study area using regional scale geological and geophysical datasets (aeromagnetic map, 1:200 000 Bedrock map form the Geological Survey of Finland; LiDAR elevation data and topographic map from National Land Survey) aiming at defining the structural framework of the area comprising (i) the major discontinuities, representing the deformation zones, and (ii) ductile trends inferred to represent foliation and lithological contacts. We verified and updated the regional interpretation with field observation data over the lithology and bedrock structure from

274 outcrops. The structural field data comprise observations over the variations in apparent foliation intensities, measured orientations of the ductile (foliation, fold, mineral lineation) and brittle (fractures and outcrop walls) structural elements. Furthermore, we observed the topological relationship of the dominant fracture sets, as well as how they control the topography of the exposed bedrock surface on highly elevated, well-outcropping areas. We defined fracture densities on outcrops and categorised the areas into seven classes (0–6) based on the number of observed fractures proportional to a reference outcrop size of 5 × 5 m to highlight the relative changes of the fracture intensity within the study area. We studied the relationship between the brittle and ductile structures to recognise any potential structural inheritances and used the resulting understanding to provide guidelines for probable fracture orientations within the areas where no outcrops are present but which still need to be covered by the bedrock-DEM modelling.

To reduce the conceptual uncertainty over the relationship between the structural characteristics (such as fracture distribution and orientation) of the deformation zones and their control on the bedrock-DEM, we generated a small-scale (2 by 5 m) 3D-photogrammetry model that provides a proxy for the large-scale morphological signatures at the bedrock surface topography underlying the sedimentary cover. The model is based on a bedrock outcrop located in the KU area, close to the inferred E-W deformation zone, characterised by a distinct sub-vertical ductile shear zone overprinted by brittle fracturing, associated with an asymmetric elongate small-scale topographic depression on the bedrock surface (Sections c–e in Figure 8). The model is based on 52 georeferenced field photographs which have been processed into point clouds, using six control points measured with a measuring band providing 2- to 3-mm precision and raster overlays using Agisoft Metashape software.

For the final part of the work, development of a structurally constrained bedrock-DEM, we used the dataset described in Putkinen et al. (2012), updated with new data (gravity, refraction seismic studies, groundwater monitor data) and models (bedrock-DEM) until December 2020 as a result from ongoing investigations by GTK. The gravity data comprise 71 survey lines, with a total length of approximately 68.5 km (20-m measurement point spacing), 32 groundwater well drilling sites, 2 intersecting seismic lines trending NE-SW and E-W and a bedrock surface DEM generated from these data using Topo to Raster and IDW interpolation methods in ArcGIS and MOVE, respectively.

Gravity data have proven successful to assess the topography of bedrock covered by sediment deposits especially for buried valley type formations (Ahokangas et al., 2020; Valjus et al., 2004), given that the density of the bedrock and the soil cover and the depth to bedrock at the end of the gravity survey lines are known. For re-interpretation of gravity data, we selected five crossing survey lines located within the area of intersection of the NNW-SSE- and E-W-trending PA and KU bedrock depressions (Figures 1 and 10). Re-interpretation involved promoting the presence of abrupt vertical breaks in the gravity data as initially recognised from over 10-m elevation contrasts between neighbouring interpretation points. For the selected lines, we conducted a 2.5-D interpretation separately for each line, using densities of 1.9 and 2.67 g/cm^3 for the *saturated* sediment layer and the underlying crystalline bedrock, respectively. Re-interpretation used the same parameters (densities and the drilling depth to bedrock) as the original model but additionally used the sharp sub-vertical breaks as input constraints.

We integrated the new gravity interpretation lines into an improved detail-scale bedrock-DEM using the orientation of the dominant brittle structures, including the 3D-photogrammetric model and the other observed outcrop morphologies as guiding constraints. Subsequently, we discuss the potential of the new approach in addressing the problematic geometries within the original bedrock-DEM as arising from the standard interpolation methods.

4 | RESULTS

4.1 | Ductile structures and dominant lithologies

The ductile structure of the study area is characterised by an open, upright, NE-SW-trending km-scale fold that deforms both the intrusive and supracrustal rocks and their ductile foliations. Foliation trends within the intrusive rocks in the southern part of the study area define a continuous, open large-scale fold. The km-scale fold within the supracrustal successions in the north (FA1 in Figure 3a) shares a similar overall geometry but is tighter and comprises smaller enclosed folds with tight to isoclinal character (FA2 and FA3 in Figure 3a). Folds within the suprcarustal rocks show a spatial association with the NNE-trending SZ1 deformation zone as indicated by the abrupt transposition of the eastern limb of fold 'FA2', as well as the pronounced NNE trends of aeromagnetic signatures and foliations in the vicinity of SZ1. Deformation zones SZ2 and SZ3 occur along the contact of the supracrustal and intrusive rocks in their northern parts, whereas towards the south they are continuous into the intrusive rocks. One further deformation zone (SZ4) within the intrusive units is sub-vertical, strikes WNW-ESE and is associated with minor sinistral shear bands observed in the field (Figure 4a).

The dominant foliation attitude is steep to vertical (Figure 3b). The foliation trends have a wide scatter, but two partially overlapping clusters are present, and these define WNW-ESE and NNW-SSE trends. These trends are representative of the strike variation on the western limb of the km-scale fold, whereas the NE-SW foliation trends corresponding to the eastern fold limb are underrepresented due to the scarcity of outcrops in the area The apparent foliation intensity within the intrusive rocks varies from very weak to moderate (Figures 4b,c), with some localised occurrences of high-strain fabrics, for example, along the contacts with the supracrustal rocks, and close to SZ3 (I and II in Figure 3, respectively). Foliations within the supracrustal rocks show an overall higher apparent intensity, although comparison with the fabrics within the intrusive rocks is not objective. The highest foliation intensities of penetrative character (Figure 4d) occur within the domain between SZ1 and SZ2, whereas high-intensity foliation within the vicinity of SZ1 is more localised in character.

4.2 | Brittle structures

Fracture density throughout the study area is generally low, averaging at two to three fractures per a reference outcrop of 5 × 5 m size (Figures 5b and 6a). However, fracturing is heterogeneous in character varying from localities with no fractures (Figure 5a) to localities with clearly denser fracturing (Figure 5c), found particularly within the KU, Jokihaara and Santavuori domains (Figure 6c–e). The triangular area

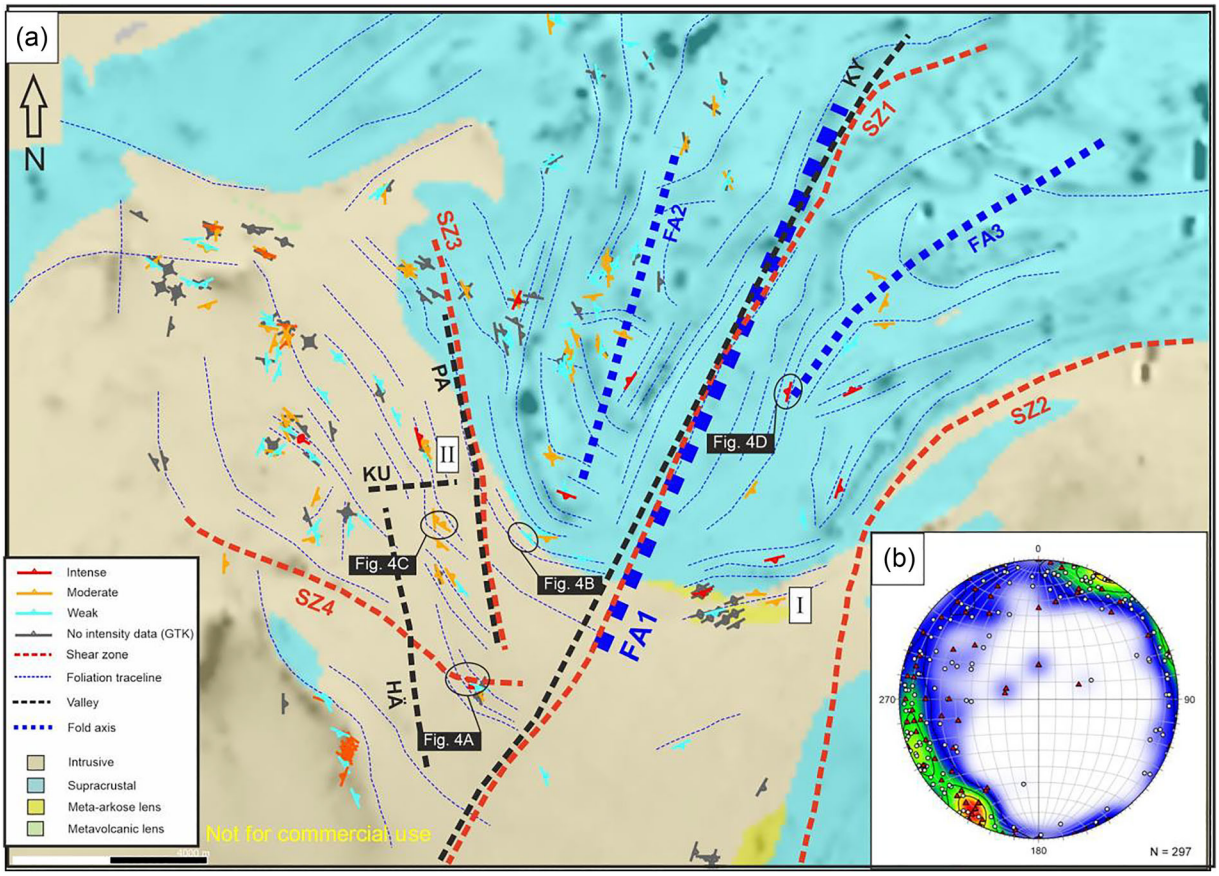

FIGURE 3 (a) Geological map representing ductile structures and apparent foliation intensity within the study area. Lithological map (1:200k) and the aeromagnetic map on the background (GTK). FA1–3 = fold axial surface traces 1–3; Ku, Kuusistonloukko; Pa, Paloluoma; SZ1–4, deformation zones 1–4; I and II location of high-strain fabrics in foliation. (b) The lower-hemisphere stereographic projection illustrates the orientation distribution of foliation data (new data = white circles, old GTK data = red triangles).

bound by SZ1 and SZ3 is characterised by an overall low fracture density. The fractures are dominantly sub-vertical, and their trends define three dominant sets: ENE-WSW, WNW-ESE and roughly N-S (Figure 6b). Additionally, sub-vertical NE–SW and sub-horizontal fractures define weaker clusters on the stereogram (Figure 6b). The weak cluster of sub-horizontal fractures is mainly due to the lack of vertical exposures available for observating sub-horizontal fractures. The sub-vertical N-S set is widely distributed, with highest densities and lateral continuity within the KU area. The N-S set is parallel to the SZ3, but on outcrops, it is a cross-cutting feature unaffected by any older fabrics. Dominant fracture sets in Santavuori and Jokihaara are controlled by the local trends of ductile foliation. Foliation trend in Santavuori ranges in N-S, NE-SW and ENE-WSW trends, and consequently, the fracture set orientations are variable. By contrast, the foliation and the foliation-parallel dominant fracture set in the Jokihaara area show more uniform WNW-ESE trends. Ductile foliation within the metaintrusive rocks of the KU area has no direct correlation with the orientation of any of the fracture sets.

Correlation between the landscape topography and the bedrock structure is well visible in the higher-elevated areas within the western part of the study area, where particularly the N-S-trending fracture set defines elongate vertical outcrops faces separating neighbouring bedrock blocks with flat and rounded upper surfaces (Figure 5d). A distinct contrast in the fracture attitude can be observed along an E-W transect crossing the Iso and Pikku Karhuvuori hills (Figure 6f): fractures within Iso Karhuvuori area define system comprising two mutually cross-cutting, 60° and 30° towards east and west-dipping fracture sets, locally defining up to 10 m-scale angular ridge and groove topographic signatures (Figures 5e and 6f). In contrast, fractures within the Pikku Karhuvuori area are all vertical to sub-vertical and have contributed to the development of 2- to 10-m-wide NNE-SSW-trending elongate depressions (Figures 5f and 6f).

4.3 | Steep to vertical slopes along the existing bedrock-DEM

We recognised a total of 50 localities (Figure 7) with more than 10-m elevation difference between neighboring interpretation points along the existing gravity investigation lines. These locations indicate the presence of steep to sub-vertical slopes within the bedrock-DEM, likely associated with the presence of pronounced bedrock fracturing within a fault or its DZ. We selected four gravity lines from the inferred intersection of the approximately E-W KU and N-S PA Valleys for re-interpretation (Figures 7 and 11). These re-interpreted profiles provide the baseline for improving the bedrock-DEMs (Section 5.3).

4.4 | The 3D-photogrammetry model

The outcrop used for the detail-scale 3D-photgrammetric modelling is characterised by a narrow E-W-trending, north-dipping shear zone

FIGURE 4 Field photos of characteristic ductile fabrics within the rocks of the study area. (a) Protomylonitic fabric associated with minor sinistral shear bands localised in pegmatite dyke along SZ4. (b) Weak foliation intensity in a porphyritic granodiorite near the contact of supracrustal and intrusive rocks. (c) Moderately foliation intensity in porphyritic granite in the vicinity of deformation zone SZ3 (see also Figure 8). View towards NE. Image width is 1.5 m. (d) Intensely foliated mica gneiss located between SZ1 and SZ2. Exact locations of the outcrops are showed in Figure 3.

which cuts porphyritic medium-grained granite (Figure 8a). Deflection of the WNW-ESE-trending ductile foliation towards the shear zone indicates that shearing had a sinistral lateral component. Coupled with the 63° E-plunging lineation observed at the shear plane, the shear zone must also have a reverse component of displacement. The shear zone is cored with a thin 2–3 cm felsic vein (not visible in Figure 8) and associated with fractures which define a structure resembling a fault with an asymmetric DZ and resulting asymmetric topographic signature. For simplicity, we use terminology typically used for faults even though we have no control on the potential brittle fault-displacement along the described structure. The southern margin of the fault is defined by a nearly continuous, steeply north-dipping master fracture which occurs in the core of the shear zone. The core of the fault is delimited by this fracture and parallel, but less continuous fractures to the north, defining an approximately 5-cm width to the fault core. Further north, within the hanging-wall of the fault, the less continuous (<1 m) and curved fractures define an anastomosing heterogeneous DZ. The DZ has its maximum width (<50 cm) in the east, and it tapers to less than 15 cm in the west.

The morphology of the observed outcrop is very clearly controlled by the fault structure (Figure 8b): The southern part of the outcrop has the highest elevation and the fault core shows the deepest erosion. The bedrock surface along the southern margin of the fault defines a very sharp step into the fault core, with some rounding on the shoulder (X in Figure 8b). The outcrop surface within the hanging wall side of the fault core shows an overall lower elevation, with a smooth increase away from the fault, with some sub-vertical segments controlled by the DZ fractures (Figure 8b–e). Complexity of the brittle deformation structures and the resulting topography are further shown by horst-like blocks (Z in Figure 8b) within the fault core domain, with flat tops elevated substantially above the fault core.

5 | INTERPRETATION AND DISCUSSION

Based on the presented results (Section 4), it is evident that the initial bedrock-DEM with smooth elevation transitions from the elevated areas to the elongate depressions (Figure 1d) does not realistically represent the true fracture-controlled character of the bedrock surface topography (Figure 8). For this reason, in the following sections, we place the observations of the brittle structures in a regional context and further use as orientation constraints for re-interpreting the gravity data and improving the bedrock-DEM, so that the new DEM better honours the structural heterogeneity of the bedrock. The improved detail-scale bedrock-DEM targets a limited area within the critical intersection of E-W and NNW-SSE bedrock depressions, but we discuss the applicability of the gained results in the scale covering the available bedrock depth data.

5.1 | The relationship between the valleys, bedrock surface depressions, regional structures and observed fracture patterns

The bedrock surface topography within the study area is uneven and characterised by several elongate bedrock depressions. Considering

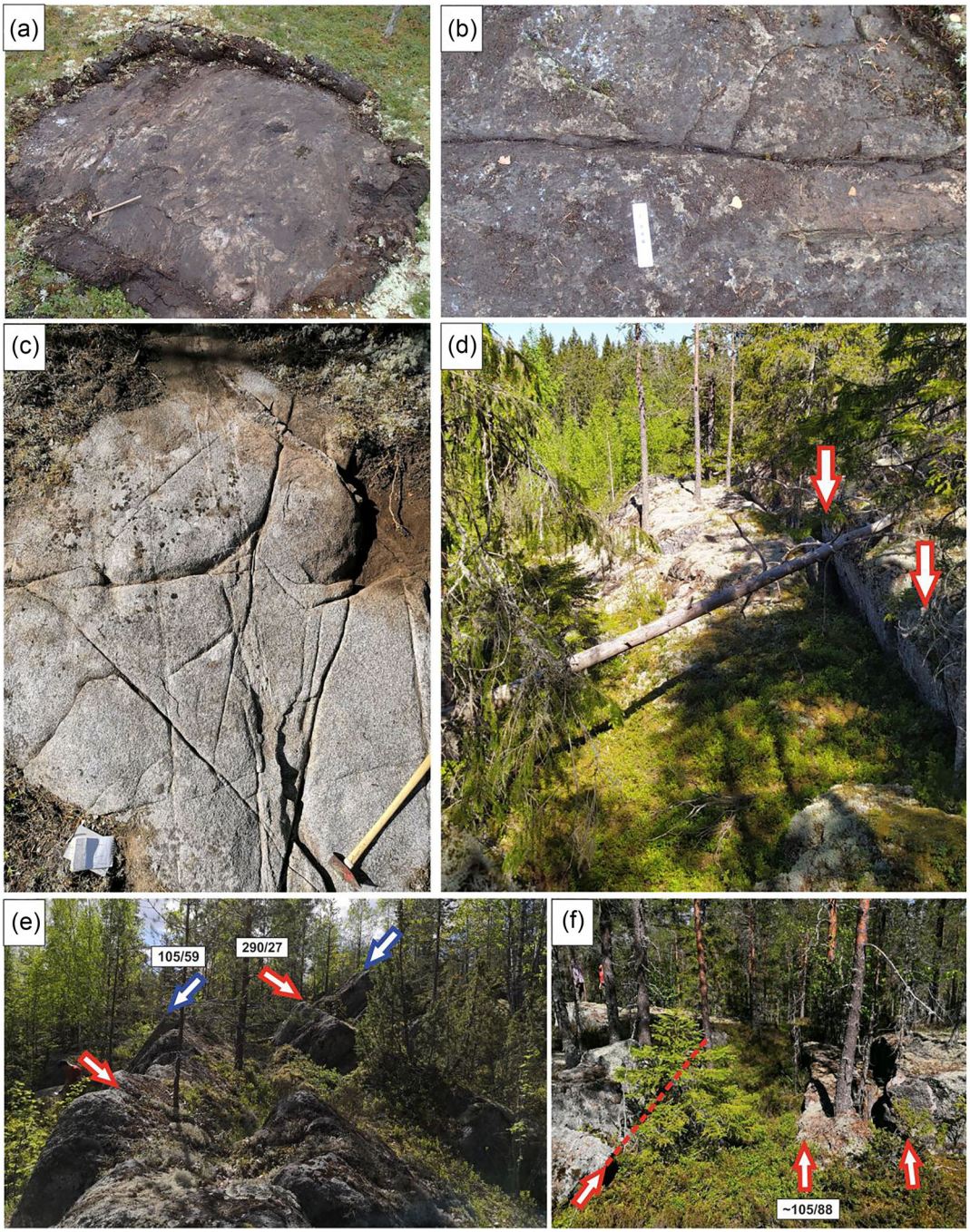

FIGURE 5 Fracture densities and topographical features of the study area. (a) Unfractured gneiss, outcrop size 6 × 8 m. Handle of the hammer pointing towards north. (b) Typical outcrop with average fracture density consisting one distinct fracture orientation in gneiss. Outcrop size 2 × 3 m view towards north. (c) High fracture density in granodiorite. Figure width is approximately 3 m. (d) Continuous N-S-trending cliffs (red arrows). View towards north. (e) Fracture-controlled cliffs forming stepped domino-style topography at Iso Karhuvuori. Red and blue arrows shows two dominant, fracture-controlled cliff orientations. View towards south. The used orientation convention is dip azimuth/dip. (f) Frequent N-S-trending low cliffs control the topography at Pikku Karhuvuori. View towards north. Location of the field photos is shown in Figure 6.

the land surface morphology, the first-order Kyröjoki river valley (KY in Figures 1c; 9), with a width of several kilometres and undefined length, is characterised by a smooth and slightly undulating surface morphology and smooth conceive-shaped sidewalls. In contrast, the smaller second-order PA and HÄ tributary valleys (PA and HÄ in Figures 1c and 9) have a more 'hilly' character along the long axis direction and also their sidewalls. The smallest high-standing valleys in the upper reach of the tributary valleys (third-order valleys in Figure 9) have a completely fracture-controlled character in the Lehtivuori and Karhuvuori area (Figure 5.).

The structural characterisation of the bedrock allows us to make a regional interpretation of the major bedrock deformation zones in the area and shed further light into the origin of the studied valleys. Considering the bedrock surface morphology, the NNE-trending major depression that spatially coincides with the KY river valley also coincides with the SZ1 deformation zone and the distinct NNE ductile structural trends of the bedrock (Figure 9). The smaller NNW-trending PA and HÄ depressions terminate against the KY depression in SSE and are recognisable 4–6 km towards NNW. The PA bedrock surface depression is a well-defined narrow (500–700 m) linear feature, which

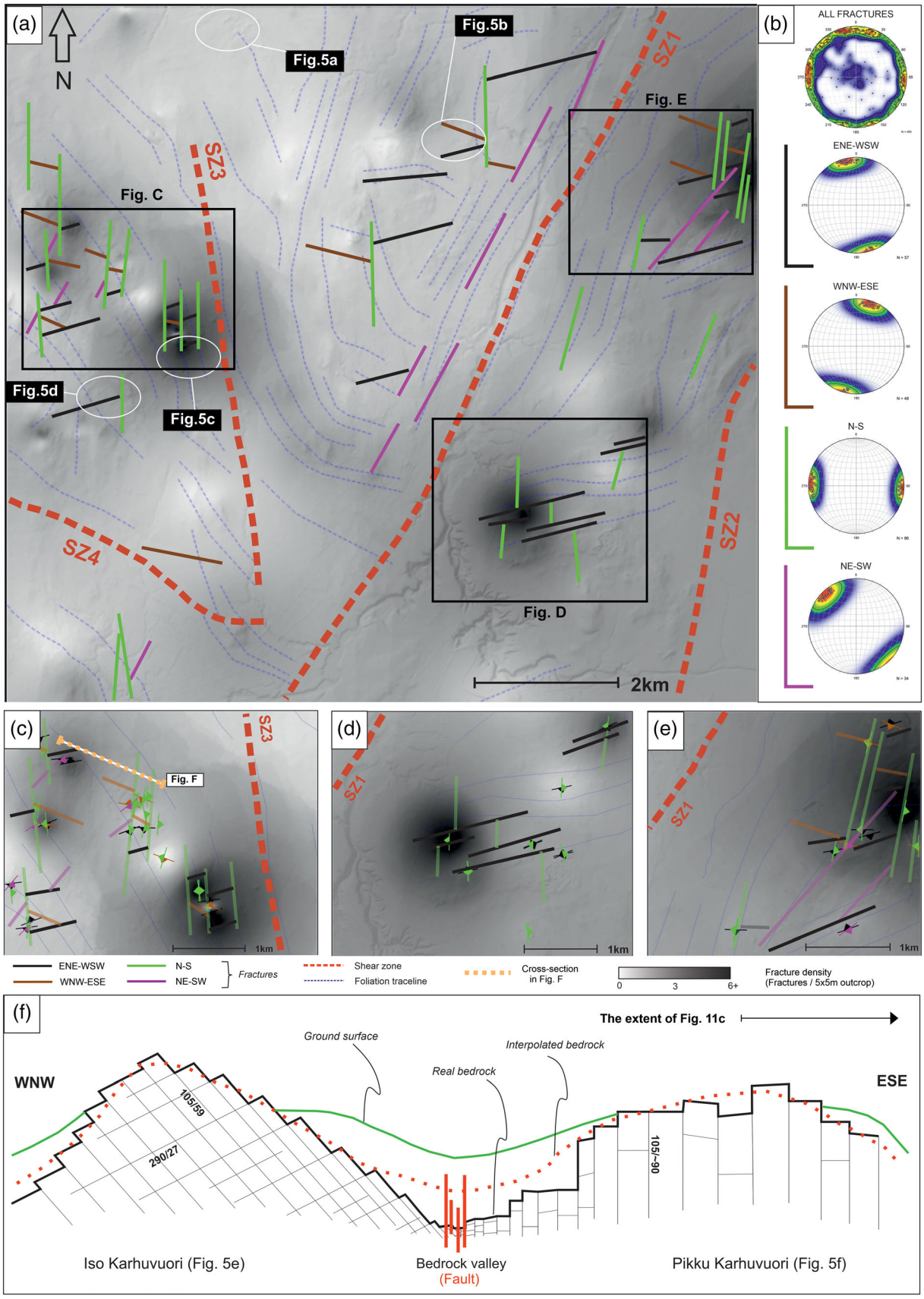

FIGURE 6 (a) An overview of the fracture densities (IDW interpolation), orientation and topological relationships within the study area. Hill-shaded ground surface topography (LiDAR) on the background (GTK). (b) Fracture orientations visualised on equal area, lower-hemisphere stereographic projections. Stereoplots from top to bottom: All fractures, ENE-WSW set (black), WNW-ESE set (brown), roughly N-S set (green) and NE–SW set (pink). (c–e) Fracture system characterisation from key areas: (c) Kuusistonloukko domain. (d) Jokihaara domain. (e) Santavuori domain. (f) Vertical cross-section across the Iso Karhuvuori and Pikku Karhuvuori hills illustrating the contrasting fracture attitudes and their relation to the landscape topographical. Black continuous line = observed and inferred outcrop topography in exposed and covered areas, red dotted line = bedrock surface after gravity data, green solid line = ground surface. Black arrow shows that reinterpreted bedrock-digital elevation models (DEMs) are located on the eastern side of the cross-section.

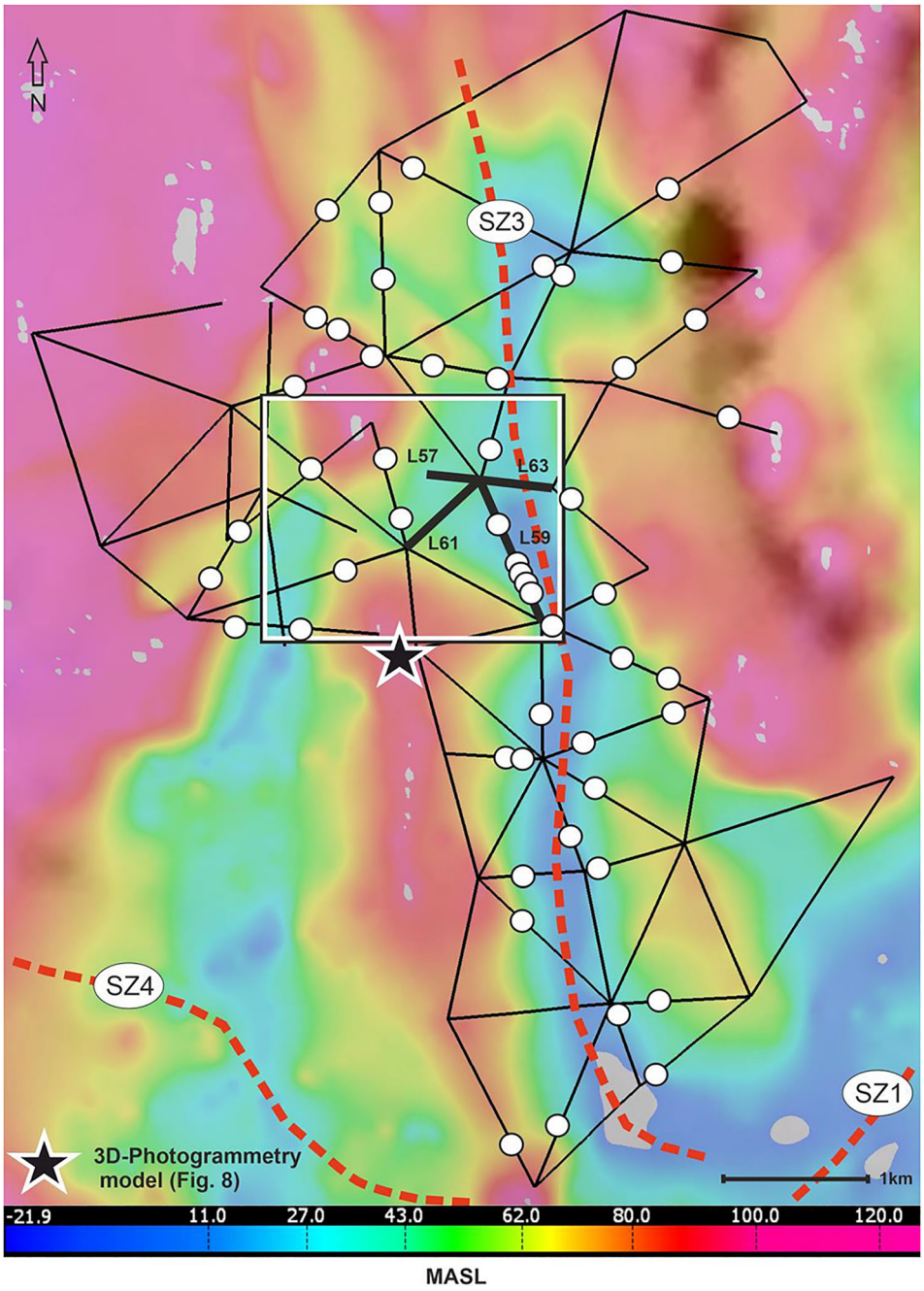

FIGURE 7 Initial bedrock-digital elevation model (DEM) (Topo to Raster & IDW interpolation). Gravity data lines are black solid lines (bolded: re-interpreted gravity lines in Figure 10). White points represent locations where are 10-m elevation contrast between the neighbouring interpretation points. The rectangular area represents the scale of the improved bedrock-DEM in Figure 11.

displays steeply dipping transitions from its central parts (at around 0 m.a.s.l.) to the areas of higher elevation on its flanks (exceeding 100 m.a.s.l.; Figures 1d, 7 and 9). By contrast, the sub-parallel HÄ depression is not equally pronounced, with more undulating margins and dominant depths ranging 10–40 m.a.s.l. along the base of the depression. The PA depression is parallel with the underlying SZ3 deformation zone, whereas no distinct bedrock structures have been recognised in association with the HÄ depression. Less continuous minor bedrock depressions comprise NNW-trending features which bound bedrock 'highs' located in-between KY and PA depressions and WNW-trending features observed on the eastern side of the KY river valley, in the northern part of the study area and within the PA depression area. One of the WNW-trending depressions apparently connects the HÄ and PA depressions, starting from the KU area in the west and continues all the way to the KY depression in the east (Figure 9). On the above basis, we categorised bedrock depression into major (first-order), minor (second-order) and connective (third-order) groups by their size, rate of matureness and prominent orientation trend and topological relationships (Figure 9), to highlight morphological differences of the bedrock depressions as successfully conducted by, for example, Hall and Gillespie (2017).

The occurrence of the approximately N-trending fractures east of the KY depression is compatible with the sinistral movement sense along the KY zone (Figure 9b). Moreover, the NW-trending fractures and the sub-parallel discontinuities along the bedrock-DEM, occurring particularly in the vicinity of the PA and HÄ depressions, were likely generated as opening-mode fractures under NW-SE paleostress conditions. The approximately E-W-trending fractures are numerous in the study area (Figure 6), but they typically abut against the longer N-S-trending ones and hence play a smaller role in governing the bedrock surface morphology. The areas with the highest relative fracture intensities occur to the east of the KY zone and at the intersection area of

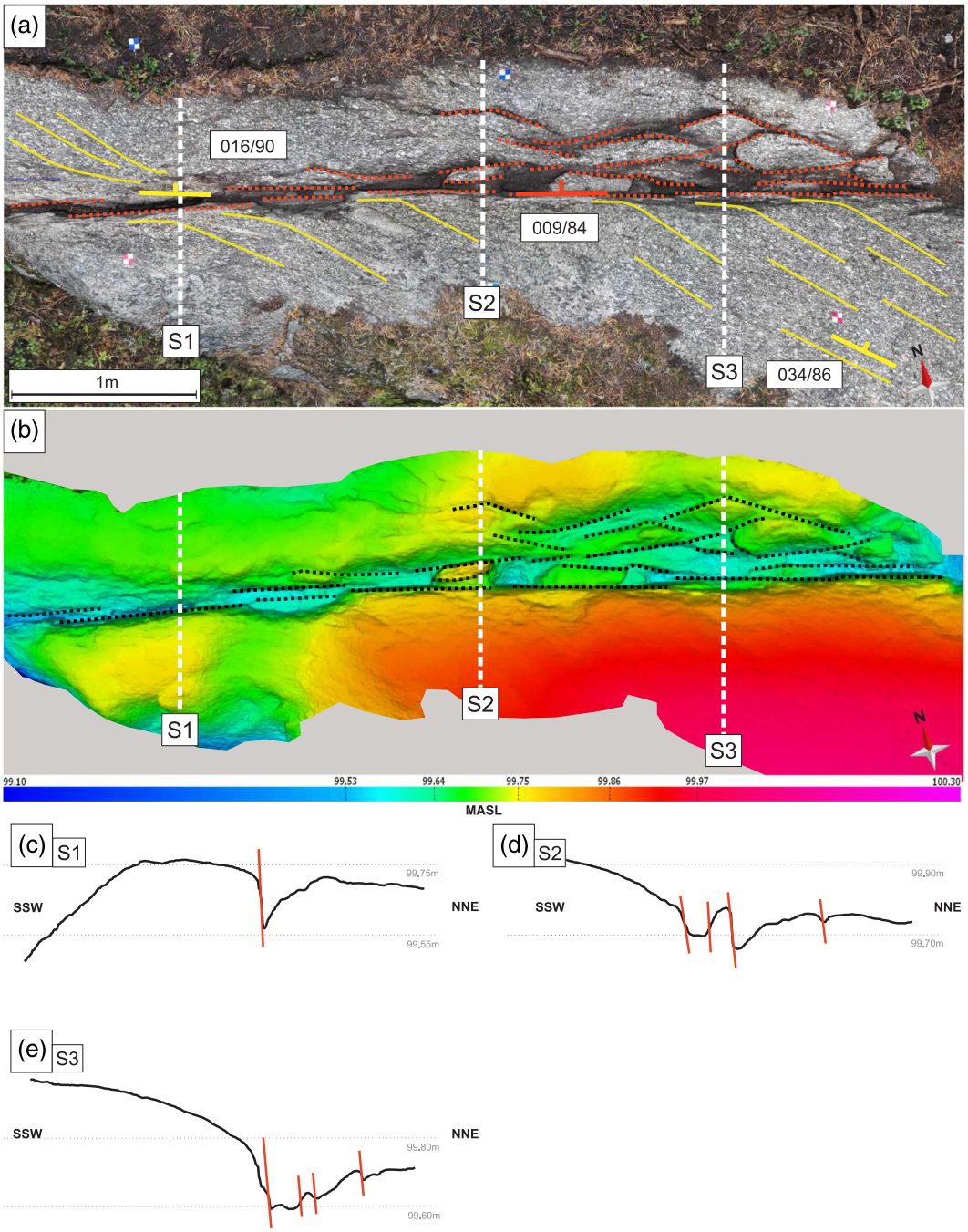

FIGURE 8 The 3D-photogrammetric model of an outcrop affected by shearing and overprinting brittle deformation, near Kuusistonloukko (for location, see Figure 7). (a) An orthophotograph of the outcrop. Foliation tracelines = yellow solid lines, fracture tracelines = red dashed lines. (b) Elevation-based colour map of the photogrammetry model, fracture tracelines as black dashed lines. (c–e) Cross-sections from west to east, respectively, in the photogrammetry model. Red lines indicating fracture-controlled slopes.

the KU, HÄ and PA zones (Figure 9b). Such spatial distribution supports that the bedrock depressions are expressions of tectonic faults or zones of brittle deformation, with surrounding DZs characterised by increased fracturing (Choi et al., 2016; Torabi et al., 2018) and heterogeneity of fracture densities (as caused by the presence of secondary slip surfaces; Ostermeijer et al., 2020). Moreover, the apparent lack of fractures may be indicative of heterogeneous DZs and the mechanical anisotropy of fault-stage structures and its controlling effect on the subsequent regional fractures (Skyttä et al., 2021).

Direct observations about fractured rocks representing zones of brittle deformation were found from two boreholes (located at the ends of the gravity line L57; Figure 11b,c), but as no drill core or drill hole video was acquired, we have no further control on the character of fracturing. However, using the recognised intimate relationship between the bedrock surface topography and the fracture system (Figure 8), we argue that the fracture density within the unexposed cores of the deformation zones underlying the bedrock depressions is much higher than within the surrounding bedrock. Consequently, the localised character of fracturing contributed not only to the bedrock surface topography but also to the hydraulic transmissivity of the bedrock, which is pronounced within the brittle deformation zones.

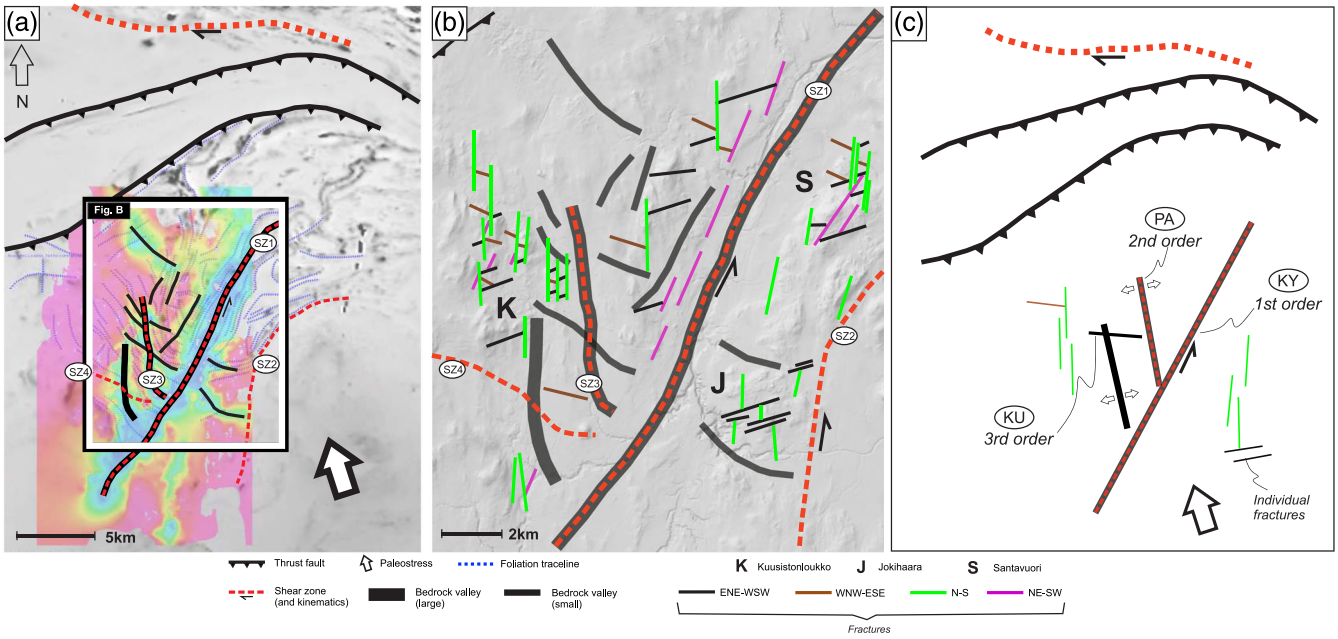

FIGURE 9 (a) Regional tectonic setting with foliation tracelines, deformation zones and bedrock depression. Initial bedrock-digital elevation model (DEM) on top of the aeromagnetic map on the background for reference. The major faults NW of the study area are drawn after bedrock map of Finland (1.200 k) by GTK. (b) Compilation of main fracture patterns with deformation zones and bedrock depressions. Colour of the fracture lineaments correspond to the colours of the fracture orientation sets in Figure 6. (c) Tectonic sketch shows the order of fracturing and generation of bedrock depressions. KU, Kuusistonloukko; KY, Kyrönjoki; PA, Paloluoma.

5.2 | Re-interpretation of selected gravity survey lines

We re-interpreted gravity survey lines L57, L59, L61 and L63, which are located within the intersection of the WNW- and NNE-trending KU and PA bedrock depressions (Figures 1d and 9). Re-interpretation of the gravity data involved replacement of steeply dipping bedrock-DEM segments in the initial bedrock surface, resulting from the >10 m elevation contrast between the neighboring gravity interpretation points, with distinct sub-vertical segments. These segments correspond to the fracture-controlled abrupt sub-vertical breaks of the bedrock surface (Figure 8), and dip constraints (80–90° dips) for these breaks were defined by the dominant fracture sets, represented in Figure 6, occurring in the vicinity (Figure 9). The dominant sub-vertical fracture attitudes within the area covered by the re-interpreted gravity lines and the bedrock-DEM (Figures 10 and 11) are supported by the change from inclined to subvertical fractures across the Iso Karhuvuori–Pikku Karhuvuori transect (Figure 6b). We infer that the ground surface depression is underlain by a bedrock surface depression which is defined by a zone of brittle bedrock deformation, and this deformation zone also acts as a boundary separating bedrock domains with contrasting fracture orientations.

Prior to the re-interpretation of the gravity data, just five such >10-m elevation contrast were recognised from lines L57, L59, L61 and L63 (all from L59; Figure 7), which were interpreted with the conventional approach placing no focus on potential structural discontinuities. Implementing the new approach, the re-interpretation introduced nine additional sub-vertical breaks that define either isolated thresholds but more commonly graben-like structures where bedrock surface locates 10–25 m lower than within the surrounding areas (Figure 10). Introducing the sub-vertical breaks but still honoring the original gravity data points, the intervening segments between the breaks became more horizontal and the overall topography more fragmented and discontinuous with respect to the initial, smoothly varying geometry. Moreover, the revised interpretation generally improved the quality of the interpretation on the selected gravimetric lines or at least resulted in equal goodness-of-fit as the conventional interpretation, as shown by the match of the interpretation curve with the Bouguer anomaly curve (Figure 9). This indicates that the new bedrock models with the distinct fracture-controlled vertical breaks, comparable with the geometry within the 3D-photogrammetry model in Figure 8, are at least as plausible as the smooth ones. Models based on gravity data, like the potential field models in general (e.g. Møller et al., 2007), quickly turn smooth in appearance if a critical depth is exceeded, but this was not the case in the present study.

The most significant structure within the re-interpreted, roughly E-W-trending line L57 is an approximately 30-m-wide and 20-m-deep depression in the eastern part of the line. The initial interpretation of the bedrock surface L59, located precisely on the bottom of the PA Valley, comprised several localised depressions, and the new interpretation further developed these into distinct graben-like features (Figure 9b). The graben in the NW part of the line is quite similar to that along line L57, whereas the presence of multiple fractures in the SE part of the line lead to a more fragmented, horst-and-graben like surface geometry. Based on re-interpretation of L61, gravimetric data are compatible with the presence of a >100-m-wide and 10- to 15-m-high depression within its central part, whereas the width of the recognised depression along line L63 is somewhat smaller.

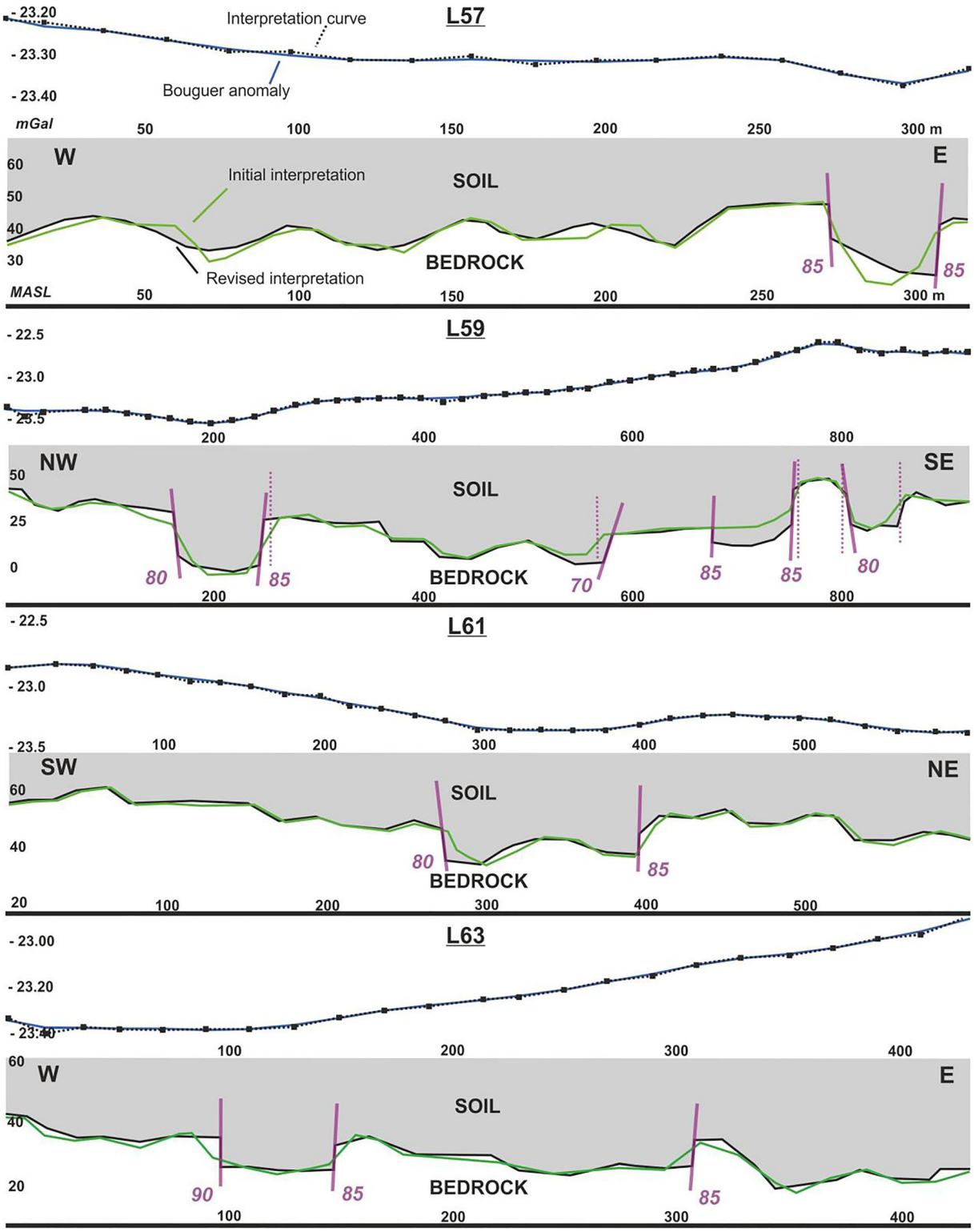

FIGURE 10 Re-interpretation of gravity data along survey lines L57, L59, L61 and L63. The fracture-controlled breaks within the bedrock-digital elevation model (DEM) marked are as purple solid lines, and the numbers indicate their approximated dips as inferred from re-interpreted bedrock surface (for location, see Figure 7). Purple dotted lines on L59 are breaks recognised before re-interpretation; equivalent with white dots in Figure 7).

5.3 | Improvement of the bedrock-DEM

The improved detail-scale bedrock-DEM is located in the central part of the study area, within the intersection of the KU, PA and HÄ bedrock depressions (Figure 11a). In generating the improved bedrock-DEM, we used bedrock surface elevation point data from (i) the re-interpreted gravity lines (L57; L59; L61; L63; Figures 7 and 10), (ii) two intersecting, NE-SW- and E-W-trending refraction seismic lines, (iii) 11 groundwater observation wells and (iv) 4–8 control points from initial bedrock-DEM to the assist modelling of large blocks (6, 7 and 8) with sparse data coverage. Moreover, we used the distinct breaks recognised in gravity re-interpretation (Figure 10) as boundaries between the blocks of contrasting elevation levels.

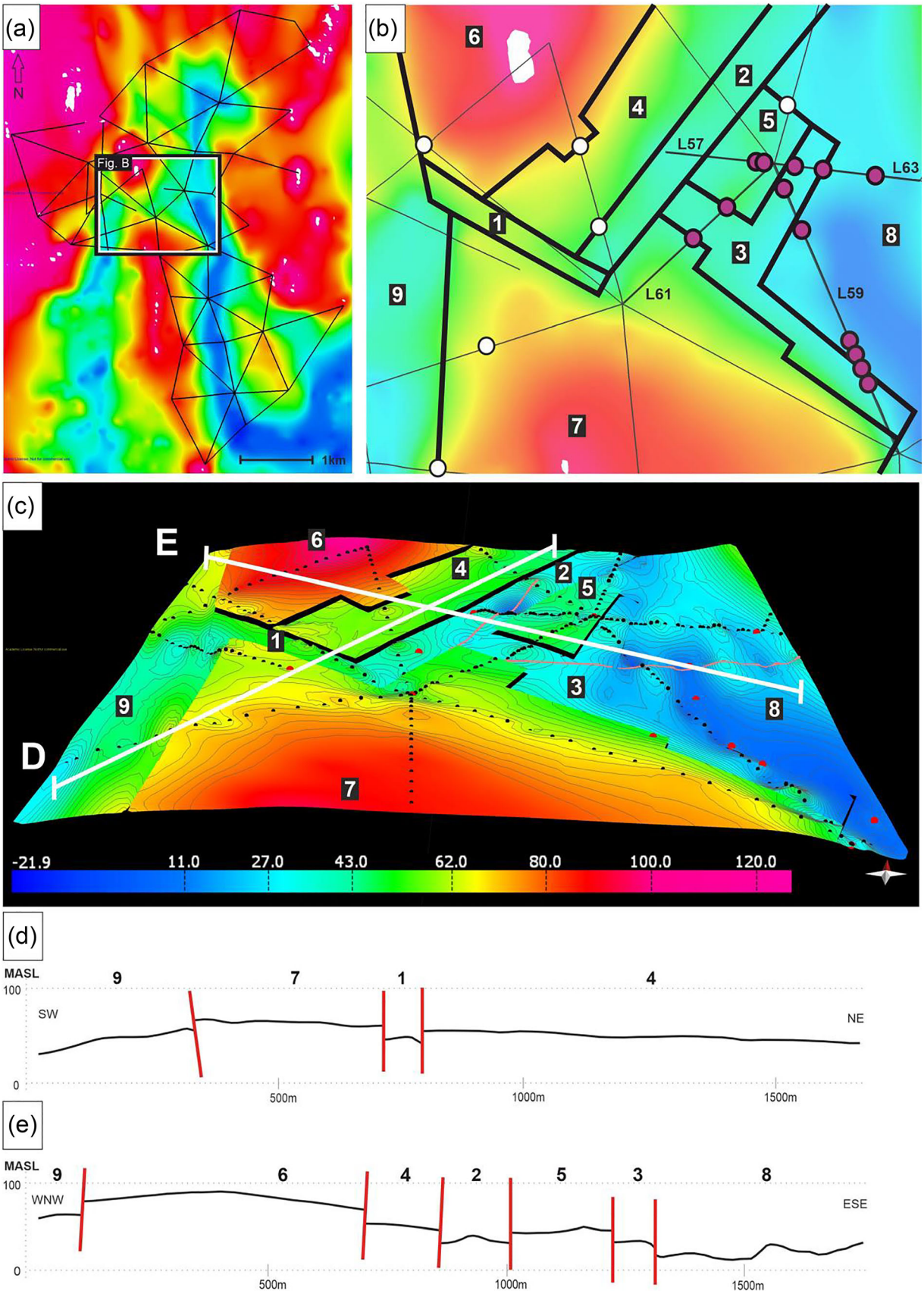

FIGURE 11 (a) Initial bedrock-digital elevation model (DEM) interpolation by GTK. Black and white frame shows the area of the improved bedrock-DEM. B) Initial bedrock-DEM from Kuusistonloukko. Thin black lines as gravity profile lines (re-interpreted L57, L59, L61 and L63 highlighted). Thick black lines represent blocks (1–9) and their boundaries modelled in panel c. White dots are abrupt breaks from initial gravity data, purple dots are abrupt breaks after re-interpretation. (c) Improved bedrock-DEM. Model comprises nine separately generated surface interpolations (blocks) using kriging method and structural anisotropy, further discussed in text. Black dots: gravity line points, red dots: groundwater monitor sites, orange line: seismic data lines. Elevation contours are at intervals of 2 m. (d) Cross-section trending NE-SW. (e) Cross-section trending WNW-ESE.

We compiled a structural interpretation developing the isolated bedrock breaks (Figures 7,10) into a network of bedrock discontinuities (fracture systems, faults) by correlating the breaks with fracture data (Section 4.2) and distinct linear slopes on the original bedrock-DEM (Figures 9 and 11b). The most pronounced slopes within the original bedrock-DEM within the whole study area trend approximately N-S (Figures 9 and 11a), whereas the detail-area additionally comprises distinct NE and WNW-trending slopes, which we consequently used to define the trends of the block boundaries. The resulting network of brittle deformation zones hence suggests that the KU zone linking the HÄ and PA depressions is not a linear feature but rather composed of approximately orthogonal, NW- and WNW-trending segments of connected bedrock structures (Figure 11b).

Using the above sub-division of bedrock blocks, we modelled each block separately using the elevation point data available for the respective blocks. For the height of the sub-vertical block boundary surfaces, we used the typical average elevation difference of 15 m observed between the opposite sides of fracture-bound bedrock depressions (Figure 10), and this elevation contrast in the revised bedrock-DEM was generated by manually lowering the elevation of boundary points on the lower block side by 15 m. We modelled the bedrock-DEM of each individual block using kriging method with a sample interval of 7.2 m. Anisotropy is utilised within blocks where specific structural trends were recognizsed: For Blocks 8 and 9, 1 and 7 and 2, we used anisotropy trends of 170–350°, 110–290° and 045–225°, respectively, whereas surface interpolation of Blocks 3–6 involved no anisotropy.

Building of the structurally controlled bedrock-DEM surface resulted in a topographic model characterised by three elevated areas which are separated from more elongate bedrock depressions by distinct sub-vertical breaks (Figure 11c–e). The overall low-elevation position interpolated for Blocks 1, 2 and 3 implies that the approximately orthogonal, NW- and WNW-trending segments of connected bedrock structures (Figure 11b) additionally define a comparable system of topographic depressions. The elevation of this 'channel' shows a systematic decrease from west to the east, reaching the lowest values within the core of the PA depression.

The bedrock depression defined by the elongate Block 1 is asymmetric, with the lowest elevations along the southern margin of the block and progressive increase in elevation towards the northern block margin (Figure 11c,d). This is comparable with the asymmetric fracture-controlled bedrock depression imaged by the photogrammetric methods (Figure 8) and supports the used approach in improving the bedrock-DEM. Our focus in this first-pass conceptual bedrock-DEM re-interpretation was placed on recognising and modelling the domains with the most pronounced elevation contrasts, that is, the 'highs and lows'. However, elevation contrasts are present also within the low-elevation blocks, which indicates that significant but smaller-scale fragmentation occurred within the bedrock depressions (Figure 11c).

5.4 | Applicability of the new approach to regional bedrock-DEM signatures

The main problems with the initial bedrock-DEM from the study area are associated with the standard interpolation approaches, which do not adequately address (i) the structural anisotropy of the of bedrock and its spatial variation and (ii) the distinct sub-vertical breaks controlled by the brittle deformation zones or larger fractures. Instead, the interpolation results in smooth and rounded shapes within the bedrock-DEM in-between the input data points, not honoring the anisotropy of controlling bedrock structures. Examples of significance for the PA-KU area include two areas in Figure 12; the area of elevated topography within the KU depression fails to represent the suggested WNW-ESE- and NE-SW-trending sub-valley system (circle 1) and the smooth rounded shapes occurring on the eastern edge of the PA depression (circle 2; Figure 12a), where the edge does not honor the sharp geometry of the bedrock topography controlled by spatial anisotropy of fracturing.

We tackled the above issues within the initial bedrock-DEM by constructing the improved detail-scale bedrock-DEM which comprises both the sub-division of the crust into structurally controlled blocks, as well as honors the controlling structural anisotropy in each block (Figure 11c). For the regional dataset, we tested the applicability of using specific structural anisotropies within interpolation of the larger bedrock-DEMs. The first interpolation (Figure 12b) highlights the structural orientation defined by the PA depression and the sub-parallel fractures and uses NNW-SSE (170–350°)-trending input anisotropy in kriging interpolation. The resulting DEM enhances the bedrock surface interpolation by sharpening the edges of the PA depression and, simultaneously, decreasing the distorted smooth shapes in the initial bedrock-DEM interpolation (circled area 2 in Figure 12). However, it also leads to partial joining of elevated areas such as Blocks 4 and 7 (Figure 11) and hence 'closes up' the E-W-trending KU depression (circled area 1 in Figure 12b). Contrastingly, using the E-W-trending anisotropy in surface interpolation, highlighting the inferred linkages between the HÄ and PA depressions, improves the bedrock surface interpolation within the KU depression, corresponding well with the improved detail-scale bedrock-DEM but simultaneously creates likely erroneous curved shapes along the linear N-S-trending bedrock depressions (circled area 2 in Figure 12c). Even if the results from interpolation using E-W-trending anisotropy correspond well with the improved detail-scale bedrock-DEM within KU depression at a general level, the model fails to recognise the WNW-ESE- and NE-SW-trending sub-valley system present in the improved detail-scale bedrock-DEM.

These examples also indicate that no single anisotropy value in surface interpolation algorithms will result geologically realistic bedrock-DEMs, but a new approach involving a dataset and an algorithm accounting also for the spatial variability in anisotropy will be needed. Moreover, the role of the major bedrock discontinuities and their contribution to the heterogeneity of the bedrock-DEM should be assessed in the studies of glaciofluvial aquifers as generating structurally controlled bedrock-DEMs may result in such local variations in the morphology of the bedrock-DEM that has major significance to the groundwater flow pathways.

5.5 | Implications of the new approach to the hydrogeology of the HÄ and PA buried valleys

Considering the flow pathways of groundwater, the revised bedrock-DEM presented in Figure 11c suggests that flow is more localised into

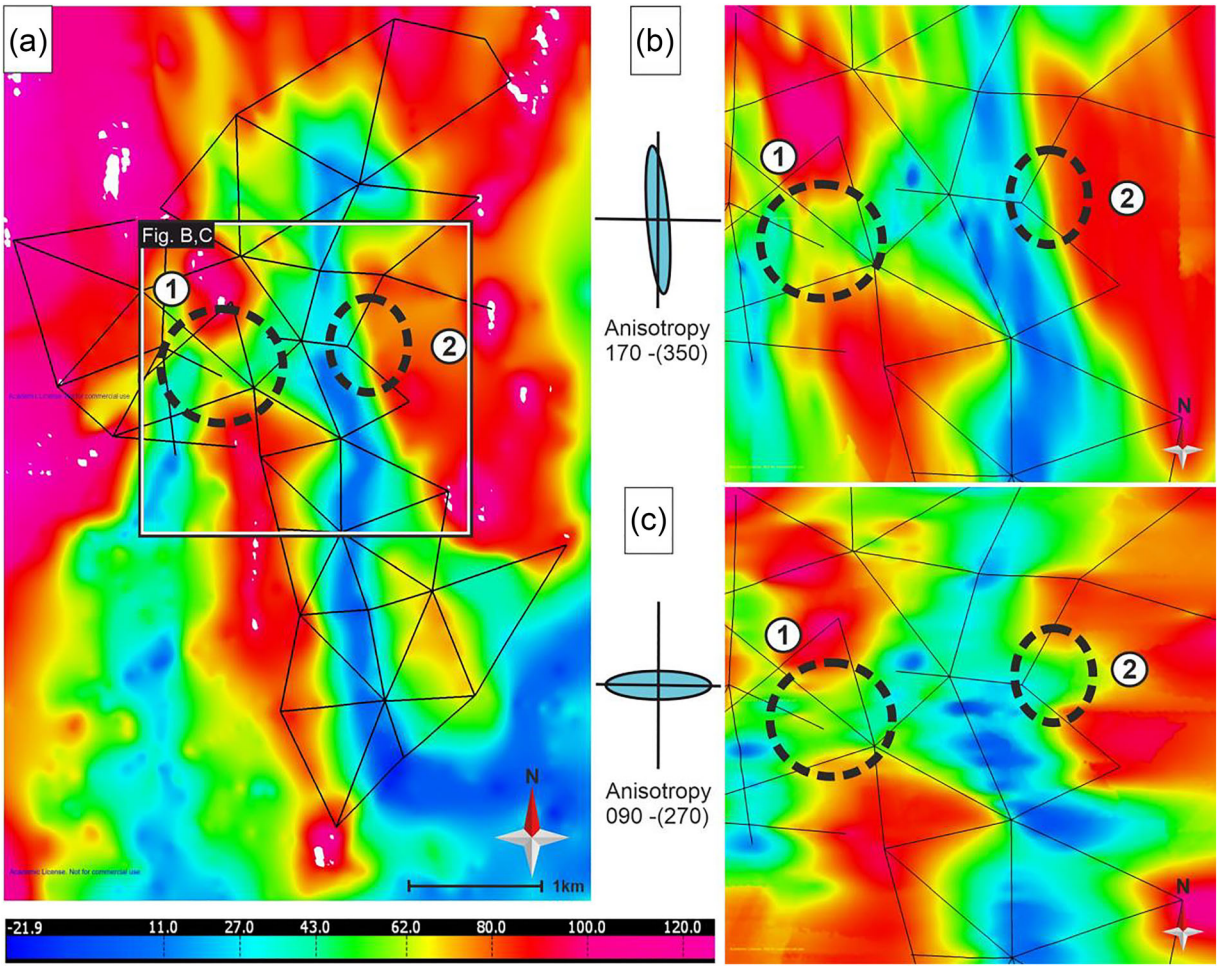

FIGURE 12 (a) The initial bedrock-digital elevation model (DEM) interpolation by GTK where marked location in the interpolations 1 and 2 are discussed in the text. (b) Conceptual bedrock-DEM interpolation using the anisotropy parallel to the orientation of the Paloluoma Valley (170/350°). (c) Bedrock-DEM interpolation with E-W-trending anisotropy parallel to the orientation of the Kuusistonloukko Valley.

structurally controlled channels of lower elevation along the bedrock surface than previously considered. As such, the mechanism is comparable with channelised fluid flow controlled by the geometry of individual structural surfaces (Brown et al., 1998). The connected pathway, 'channel', from HÄ to PA depressions is particularly important as it defines a suitable site of deposition for the well-conductive glaciofluvial sediments (middle sand) considered responsible for the hydrogeological connectivity between these two depressions (Putkinen et al., 2012). Moreover, distinct bedrock depressions comparable with, for example, the deepest parts of the asymmetric depression in Figure 8 may host even coarser sediments with higher permeability and further improve the channelizing effect.

The recognised fracture signatures of the bedrock, associated with the elongate bedrock depressions and abrupt breaks along the bedrock-DEM (Figures 8, 9 and 11), suggest that not only the bedrock depressions but also the fracture zones within the underlying bedrock act as fluid pathways (Faulkner et al., 2010). The linkage of the Häjynluoma, PA and KU deformation zones and the resulting network of fracture zones likely contributed to the groundwater flow within the bedrock, with potential development of channelised flow pathways also within the bedrock (Cox, 1999; Dimmen et al., 2017; Micklethwaite et al., 2015; Peacock et al., 2017; Peacock et al., 2018; Seebeck et al., 2014). Previous studies have shown that the hydrogeology system of the HÄ-PA buried valleys is strongly controlled by the watershed-scale bedrock surface topography and the local bedrock topography and the resulting groundwater channelisation (Figure 11c) and also by the hydraulic properties of the bedrock and the sediments (Putkinen et al., 2020; Putkinen et al., 2012; Rashid et al., 2020). We infer that the groundwater flow route from the recharge region downward to the buried valleys selectively utilises the material of the highest conductivity—be it the sediment cover or the fractured bedrock within the contact zone of the bedrock-sediment contact.

6 | CONCLUSIONS

Weathering and erosion over the last 1.5 Ga have exploited bedrock deformation zones to form valleys at Kurikka that today hold glaciofluvial sediments up to 100 m thick, hosting major glaciofluvial aquifers. Re-interpretation of the gravity data used for imaging and modelling bedrock surface topography shows that the margins of the elongated bedrock depressions are sharp in geometry, reflecting their fracture-controlled character. Mapping structural anisotropy in bedrock exposures and gravity data allowed the development of improved DEMs of the bedrock surface. Vertical fracture zones connect the surface aquifer to deep groundwater. Furthermore, previously unrecognised pathways for water movement were recognised along trench floors. Modelling groundwater movement in crystalline

bedrock requires an understanding of structural anisotropy and buried bedrock topography.

ACKNOWLEDGEMENTS

Eemi Ruuska has been funded by Maa- ja Vesiteksiikan Tuki Ry (13-7820-39), alongside field work funding provided by municipal waterworks Kurikan Vesihuolto Oy and Vaasan Vesi.

DATA AVAILABILITY STATEMENT

The data that support the findings of this study are available from the corresponding author upon reasonable request.

ORCID

Eemi Ruuska https://orcid.org/0000-0001-5922-2538

REFERENCES

Ahokangas, E., Mäkinen, J., Artimo, A., Pasanen, A. & Vanhala, H. (2020) Interlobate esker aquifer characterization by high resolution seismic reflection method with landstreamer in SW Finland. *Journal of Applied Geophysics*, 177, 104014. Available from: https://doi.org/10.1016/j.jappgeo.2020.104014

Barr, I.D. & Lovell, H. (2014) A review of topographic controls on moraine distribution. *Geomorphology*, 226, 44–64. Available from: https://doi.org/10.1016/j.geomorph.2014.07.030

Benn, D.I. & Evans, D.J.A. (2010) *Glaciers & glaciation*, 2nd edition, London: Hodder Arnold, p. 801. Available from: https://doi.org/10.4324/9780203785010

Boulton, G.S. (1986) Push-moraines and glacier-contact fans in marine and terrestrial environments. *Sedimentology*, 33(5), 677–698. Available from: https://doi.org/10.1111/j.1365-3091.1986.tb01969.x

Boulton, G.S., Dongelmans, P., Punkari, M. & Broadgate, M. (2001) Palaeoglaciology of an ice sheet through a glacial cycle: the European ice sheet through the Weichselian. *Quaternary Science Reviews*, 20(4), 591–625. Available from: https://doi.org/10.1016/S0277-3791(00)00160-8

Brown, S., Caprihan, A. & Hardy, R. (1998) Experimental observation of fluid flow channels in a single fracture: journal of geophysical research: solid. *Earth*, 103(B3), 5125–5132. Available from: https://doi.org/10.1029/97jb03542

Burbank, D.W. & Fort, M.B. (1985) Bedrock control on glacial limits: examples from the Ladakh and Zanskar ranges, North-Western Himalaya, India. *Journal of Glaciology*, 31(108), 143–149. Available from: https://doi.org/10.3189/s0022143000006389

Cassidy, R., Comte, J.C., Nitsche, J., Wilson, C., Flynn, R. & Ofterdinger, U. (2014) Combining multi-scale geophysical techniques for robust hydro-structural characterisation in catchments underlain by hard rock in post-glacial regions. *Journal of Hydrology*, 517, 715–731. Available from: https://doi.org/10.1016/j.jhydrol.2014.06.004

Childs, C., Manzocchi, T., Walsh, J.J., Bonson, C.G., Nicol, A. & Schöpfer, M.P.J. (2009) A geometric model of fault zone and fault rock thickness variations. *Journal of Structural Geology*, 31(2), 117–127. Available from: https://doi.org/10.1016/j.jsg.2008.08.009

Choi, J.H., Edwards, P., Ko, K. & Kim, Y.S. (2016) Definition and classification of fault damage zones: a review and a new methodological approach. *Earth-Science Reviews*, 152, 70–87. Available from: https://doi.org/10.1016/j.earscirev.2015.11.006

Chopin, F., Korja, A., Nikkilä, K., Hölttä, P., Korja, T., Zaher, M.A. et al. (2020) The Vaasa migmatitic complex (Svecofennian Orogen, Finland): buildup of a LP-HT dome during Nuna assembly. *Tectonics*, 39(3), e2019TC005583. Available from: https://doi.org/10.1029/2019TC005583

Cox, S.F. (1999) Deformational controls on the dynamics of fluid flow in mesothermal gold systems. *Geological Society, London*, Special Publications, 155(1), 123 LP – 140. Available from: https://doi.org/10.1144/GSL.SP.1999.155.01.10

DesRoches, A., Danielescu, S. & Butler, K. (2014) Contrôles structuraux sur les écoulements souterrains d'un aquifère de roche fracturée au droit d'une région agricole au nord-ouest de New Brunswick au Canada. *Hydrogeology Journal*, 22(5), 1067–1086. Available from: https://doi.org/10.1007/s10040-014-1134-0

Dimmen, V., Rotevatn, A., Peacock, D.C.P., Nixon, C.W. & Nærland, K. (2017) Quantifying structural controls on fluid flow: insights from carbonate-hosted fault damage zones on the Maltese islands. *Journal of Structural Geology*, 101, 43–57. Available from: https://doi.org/10.1016/j.jsg.2017.05.012

Faulkner, D.R., Jackson, C.A.L., Lunn, R.J., Schlische, R.W., Shipton, Z.K., Wibberley, C.A.J. & Withjack, M.O. (2010) A review of recent developments concerning the structure, mechanics and fluid flow properties of fault zones. *Journal of Structural Geology*, 32(11), 1557–1575. Available from: https://doi.org/10.1016/j.jsg.2010.06.009

Gao, C. (2011) Buried bedrock valleys and glacial and subglacial meltwater erosion in southern Ontario, Canada. *Canadian Journal of Earth Sciences*, 48(5), 801–818. Available from: https://doi.org/10.1139/e10-104

Gibbard, P.L. & Lewin, J. (2016) Filling the North Sea Basin: Cenozoic sediment sources and river styles. *Geologica Belgica*, 19(3-4), 201–217. Available from: https://doi.org/10.20341/gb.2015.017

Gleeson, T. & Novakowski, K. (2009) Identifying watershed-scale barriers to groundwater flow. *Lineaments in the Canadian Shield: GSA Bulletin*, 121(3-4), 333–347. Available from: https://doi.org/10.1130/B26241.1

Godbout, P., Lamothe, M. & Larocque, M. (2011). Hydrostratigraphy and quaternary geology of the Bécancour area watersheds, Québec.

Hall, A.M. & Gillespie, M.R. (2017) Fracture controls on valley persistence: the cairngorm granite pluton, Scotland. *International Journal of Earth Sciences*, 106(6), 2203–2219. Available from: https://doi.org/10.1007/s00531-016-1423-z

Hall, A.M., Putkinen, N., Hietala, S., Lindsberg, E. & Holma, M. (2021) Ultra-slow cratonic denudation in Finland since 1.5 Ga indicated by tiered unconformities and impact structures. *Precambrian Research*, 352, 106000. Available from: https://doi.org/10.1016/j.precamres.2020.106000

Kempton, J.P., Johnson, W.H., Heigold, P.C. & Cartwright, K. (1991) Mahomet bedrock valley in east-central Illinois: topography, glacial drift stratigraphy, and hydrogeology. In: Melhorn, W.N. & Kempton, J.P. (Eds.) *Geology and hydrogeology of the Teays-Mahomet bedrock valley system*, Vol. 258. Colorado: Geological Society of America. Available from: https://doi.org/10.1130/SPE258-p91

Kim, Y.S., Peacock, D.C.P. & Sanderson, D.J. (2004) Fault damage zones. *Journal of Structural Geology*, 26(3), 503–517. Available from: https://doi.org/10.1016/j.jsg.2003.08.002

Korme, T., Acocella, V. & Abebe, B. (2004) The role of pre-existing structures in the origin, propagation and architecture of faults in the Main Ethiopian Rift. *Gondwana Research*, 7(2), 467–479. Available from: https://doi.org/10.1016/S1342-937X(05)70798-X

Lahtinen, R., Huhma, H., Sipilä, P. & Vaarma, M. (2017) Geochemistry, U-Pb geochronology and Sm-Nd data from the Paleoproterozoic Western Finland supersuite—a key component in the coupled Bothnian oroclines. *Precambrian Research*, 299, 264–281. Available from: https://doi.org/10.1016/j.precamres.2017.07.025

Lehtonen, M.I., Kujala, H., Kärkkäinen, N., Lehtonen, A., Mäkitie, H., Mänttäri, I., Virransalo, P. & Vuokko, J. (2005) Etelä-Pohjanmaan liuskealueen kallioperä. Summary: pre-Quaternary rocks of the South Ostrobothnian Schist Belt.

Lipponen, A. (2006) Topographical, structural and geophysical characterization of fracture zones: implications for groundwater flow and vulnerability. In: Heikinheimo, O., Kerminen, V.-M., Mattila, J., Laiho, R., Huttula, T. & Raciborski, K. (Eds.) *Monographs of the boreal environment research 25*. Finland: Finnish Environment Institute, p. 62.

Lovell, H., Stokes, C.R. & Bentley, M.J. (2011) A glacial geomorphological map of the Seno Skyring-Seno Otway-Strait of Magellan region, southernmost Patagonia. *Journal of Maps*, 7(1), 318–339. Available from: https://doi.org/10.4113/jom.2011.1156

Mancktelow, N.S. & Pennacchioni, G. (2005) The control of precursor brittle fracture and fluid-rock interaction on the development of single and paired ductile shear zones. *Journal of Structural Geology*, 27(4), 645–661. Available from: https://doi.org/10.1016/j.jsg.2004.12.001

Micklethwaite, S., Ford, A., Witt, W. & Sheldon, H.A. (2015) The where and how of faults, fluids and permeability—insights from fault stepovers, scaling properties and gold mineralisation. *Geofluids*, 15(1-2), 240–251. Available from: https://doi.org/10.1111/gfl.12102

Møller, M.J., Olsen, H., Ploug, C., Strykowski, G. & Hjorth, H. (2007) Gravity field separation and mapping of buried quaternary valleys in Lolland. *Denmark Using Old Geophysical Data*, 43(2), 330–337. Available from: https://doi.org/10.1016/j.jog.2006.09.021

Nikkilä, K., Mänttäri, I., Nironen, M., Eklund, O. & Korja, A. (2016) Three stages to form a large batholith after terrane accretion – An example from the Svecofennian orogen. *Precambrian Research*, 281, 618–638. Available from: https://doi.org/10.1016/j.precamres.2016.06.018

Nironen, M., Elliott, B.A. & Rämö, O.T. (2000) 1.88-1.87 Ga post-kinematic intrusions of the central Finland granitoid complex: a shift from C-type to A-type magmatism during lithospheric convergence. *Lithos*, 53(1), 37–58. Available from: https://doi.org/10.1016/S0024-4937(00)00007-4

Okko, M. (1962) *On the development of the first Salpausselkä, vol. 202. West of Lahti*. Bulletin de la commission geologique de Finlande, p. 162.

Ostermeijer, G.A., Mitchell, T.M., Aben, F.M., Dorsey, M.T., Browning, J., Rockwell, T.K. et al. (2020) Damage zone heterogeneity on seismogenic faults in crystalline rock; a field study of the Borrego Fault, Baja California. *Journal of Structural Geology*, 137, 104016. Available from: https://doi.org/10.1016/j.jsg.2020.104016

Pääkkönen, V. (1966) On the geology and mineralogy of the occurrence of native antimony at Seinäjoki, Finland. *Bulletin*, 225, 70.

Palmu, J.-P. (1999) Sedimentary environment of the Second Salpausselkä ice marginal deposits in the Karkkila-Loppi area in southwestern Finland /: Sedimentary environment of the Second Salpausselkä ice marginal deposits in the Karkkila-Loppi area in southwestern Finland.

Peacock, D.C.P., Dimmen, V., Rotevatn, A. & Sanderson, D.J. (2017) A broader classification of damage zones. *Journal of Structural Geology*, 102, 179–192. Available from: https://doi.org/10.1016/j.jsg.2017.08.004

Peacock, D.C.P., Sanderson, D.J. & Rotevatn, A. (2018) Relationships between fractures. *Journal of Structural Geology*, 106, 41–53. Available from: https://doi.org/10.1016/j.jsg.2017.11.010

Pitkäranta, R. (2009) Lithostratigraphy and age estimations of the Pleistocene erosional remnants near the centre of the Scandinavian glaciations in western Finland. *Quaternary Science Reviews*, 28(1-2), 166–180. Available from: https://doi.org/10.1016/j.quascirev.2008.10.003

Pizzi, A. & Galadini, F. (2009) Pre-existing cross-structures and active fault segmentation in the northern-central Apennines (Italy). *Tectonophysics*, 476, 304–319. Available from: https://doi.org/10.1016/j.tecto.2009.03.018

Pokki, J., Kohonen, J., Lahtinen, R., Rämö, O.T. & Andersen, T. (2013) *Petrology and provenance of the mesoproterozoic Satakunta formation*, vol. 204. SW Finland: Tutkimusraportti-Geologian Tutkimuskeskus, pp. 1–61.

Putkinen, N., Eyles, N., Putkinen, S., Ojala, A.E., Palmu, J.P., Sarala, P. et al. (2017) High-resolution LiDAR mapping of glacial landforms and ice stream lobes in Finland. *Bulletin of the Geological Society of Finland*, 89, 64–81. Available from: https://doi.org/10.17741/bgsf/89.2.001

Putkinen, N., Putkinen, S. & Valjus, T. (2012) Kurikan Kuusistonloukon pohjavesialueen geologinen rakenneselvitys.

Putkinen, N., Ross, M., Hall, A.M. & Lindsberg, E. (2020) A valley-fill sequence in old bedrock valleys provide evidence for complex cyclial interlobate and ice-marginal fluctuations during the last deglaciation in west-central Finland.

Rashid, A.B., Lefebvre, R., Ballard, J.-M., Ross, M. & Putkinen, N. (2020) Towards quantifying groundwater resources of the Paloluoma valley in west-central Finland. In Groundwater Availability and Sustainability Studies: Advances, Methods and Approaches, GSA 2020 Connects Online, p. 3–5.

Richard, S.K. & Chesnaux, R. (2014) Field evidence of hydraulic connections between bedrock aquifers and overlying granular aquifers: examples from the Grenville Province of the Canadian Shield. *Hydrogeology Journal*, 22(8), 1889–1904. Available from: https://doi.org/10.1007/s10040-014-1183-4

Ross, M., Parent, M. & Lefebvre, R. (2005) 3D geologic framework models for regional hydrogeology and land-use management: a case study from a Quaternary basin of southwestern Quebec, Canada. *Hydrogeology Journal*, 13(5-6), 690–707. Available from: https://doi.org/10.1007/s10040-004-0365-x

Russell, H.A.J, Hinton, M.J., van der Kamp, G. & Sharpe, D.R. (2004) Earth sciences sector general information product 27 an overview of the architecture, sedimentology and hydrogeology of buried-valley aquifers in Canada. An overview of the architecture, sedimentology and Natural Resources Canada, p. 26–33.

Sanderson, D.J. & Peacock, D.C.P. (2019) Line sampling of fracture swarms and corridors. *Journal of Structural Geology*, 122, 27–37. Available from: https://doi.org/10.1016/j.jsg.2019.02.006

Seebeck, H., Nicol, A., Walsh, J.J., Childs, C., Beetham, R.D. & Pettinga, J. (2014) Fluid flow in fault zones from an active rift. *Journal of Structural Geology*, 62, 52–64. Available from: https://doi.org/10.1016/j.jsg.2014.01.008

Shreve, R.L. (1972) Movement of water in glaciers. *Journal of Glaciology*, 11(62), 205–214. Available from: https://doi.org/10.3189/s002214300002219x

Shreve, R.L. (1985) Late Wisconsin ice-surface profile calculated from esker paths and types, Katahdin esker system, Maine. *Quaternary Research*, 23(1), 27–37. Available from: https://doi.org/10.1016/0033-5894(85)90069-9

Skyttä, P., Kinnunen, J., Palmu, J.P. & Korkka-Niemi, K. (2015) Bedrock structures controlling the spatial occurrence and geometry of 1.8Ga younger glacifluvial deposits—example from first Salpausselkä, southern Finland. *Global and Planetary Change*, v. 135, 66–82. Available from: https://doi.org/10.1016/j.gloplacha.2015.10.007

Skyttä, P., Ovaskainen, N., Nordb, N. & Engstr, J. (2021) Fault-induced mechanical anisotropy and its effects on fracture patterns in crystalline rocks Pietari Skytta. *Journal of Structural Geology*, 146, 104304. Available from: https://doi.org/10.1016/j.jsg.2021.104304

Skyttä, P. & Torvela, T. (2018) Brittle reactivation of ductile precursor structures: the role of incomplete structural transposition at a nuclear waste disposal site, Olkiluoto, Finland. *Journal of Structural Geology*, 116, 253–259. Available from: https://doi.org/10.1016/j.jsg.2018.06.009

Steelman, C.M., Arnaud, E., Pehme, P. & Parker, B.L. (2018) Geophysical, geological, and hydrogeological characterization of a tributary buried bedrock valley in southern Ontario. *Canadian Journal of Earth Sciences*, 55(7), 641–658. Available from: https://doi.org/10.1139/cjes-2016-0120

Stephens, M.B., Follin, S., Petersson, J., Isaksson, H., Juhlin, C. & Simeonov, A. (2015) Review of the deterministic modelling of deformation zones and fracture domains at the site proposed for a spent nuclear fuel repository, Sweden, and consequences of structural anisotropy. *Tectonophysics*, 653, 68–94. Available from: https://doi.org/10.1016/j.tecto.2015.03.027

Sugden, D.E. & John, B.S. (1976) *Glaciers and landscape: a geomorphological approach*. London: Edward Arnold.

Torabi, A., Alaei, B. & Ellingsen, T.S.S. (2018) Faults and fractures in basement rocks, their architecture, petrophysical and mechanical properties. *Journal of Structural Geology*, 117, 256–263. Available from: https://doi.org/10.1016/j.jsg.2018.07.001

Vaarma, M. & Kähkönen, Y. (1994) Geochemistry of the Paleoproterozoic metavolcanic rocks at Evijärvi, western Finland. In: Niironen, M. & Kähkönen, Y. (Eds.) *Geochemistry of proterozoic supracrustal rocks in Finland, Geol. Surv. Finland, Spec. Pap, 19. Espoo*, Finland: Geological Survey of Finland, pp. 47–59.

Valjus, T., Breilin, O., Vanhala, H. & Lehtimäki, J. (2004) Detailed Geophysical Study of Glaciofluvial Aquifer at Kempele, Western Finland. Available from: https://doi.org/10.3997/2214-4609-pdb.10.P022

How to cite this article: Ruuska, E., Skyttä, P., Putkinen, N. & Valjus, T. (2023) Contribution of bedrock structures to the bedrock surface topography and groundwater flow systems within deep glaciofluvial aquifers in Kurikka, Western Finland. *Earth Surface Processes and Landforms*, 1–18. Available from: https://doi.org/10.1002/esp.5602